

Hydrocarbons Are Essential for Optimal Cell Size, Division, and Growth of Cyanobacteria¹[OPEN]

David J. Lea-Smith*, Maite L. Ortiz-Suarez, Tchern Lenn, Dennis J. Nürnberg², Laura L. Baers, Matthew P. Davey, Lucia Parolini, Roland G. Huber, Charles A.R. Cotton², Giulia Mastroianni, Paolo Bombelli, Petra Ungerer, Tim J. Stevens, Alison G. Smith, Peter J. Bond, Conrad W. Mullineaux, and Christopher J. Howe

Department of Biochemistry, University of Cambridge, Cambridge CB2 1QW, United Kingdom (D.J.L.-S., L.L.B., C.A.R.C., P.B., C.J.H.); Centre for Molecular Science Informatics, Department of Chemistry, University of Cambridge, Cambridge CB2 1EW, United Kingdom (M.L.O.-S., P.J.B.); School of Biological and Chemical Sciences, Queen Mary University of London, London E1 4NS, United Kingdom (T.L., D.J.N., G.M., P.U., C.W.M.); Department of Plant Sciences, University of Cambridge, Cambridge CB2 3EA, United Kingdom (M.P.D., A.G.S.); Department of Physics, University of Cambridge, Cambridge CB3 0HE, United Kingdom (L.P.); Bioinformatics Institute, A*STAR, Singapore 138671 (R.G.H., P.J.B.); MRC Laboratory of Molecular Biology, Cambridge CB2 0QH, United Kingdom (T.J.S.); and National University of Singapore, Department of Biological Sciences, Singapore 117543 (P.J.B.)

ORCID IDs: 0000-0002-2980-9749 (M.L.O.-S.); 0000-0002-5827-4616 (T.L.); 0000-0001-6511-5704 (A.G.S.); 0000-0003-2900-098X (P.J.B.); 0000-0001-7194-9916 (C.W.M.).

Cyanobacteria are intricately organized, incorporating an array of internal thylakoid membranes, the site of photosynthesis, into cells no larger than other bacteria. They also synthesize C15-C19 alkanes and alkenes, which results in substantial production of hydrocarbons in the environment. All sequenced cyanobacteria encode hydrocarbon biosynthesis pathways, suggesting an important, undefined physiological role for these compounds. Here, we demonstrate that hydrocarbon-deficient mutants of *Synechococcus* sp. PCC 7002 and *Synechocystis* sp. PCC 6803 exhibit significant phenotypic differences from wild type, including enlarged cell size, reduced growth, and increased division defects. Photosynthetic rates were similar between strains, although a minor reduction in energy transfer between the soluble light harvesting phycobilisome complex and membrane-bound photosystems was observed. Hydrocarbons were shown to accumulate in thylakoid and cytoplasmic membranes. Modeling of membranes suggests these compounds aggregate in the center of the lipid bilayer, potentially promoting membrane flexibility and facilitating curvature. In vivo measurements confirmed that *Synechococcus* sp. PCC 7002 mutants lacking hydrocarbons exhibit reduced thylakoid membrane curvature compared to wild type. We propose that hydrocarbons may have a role in inducing the flexibility in membranes required for optimal cell division, size, and growth, and efficient association of soluble and membrane bound proteins. The recent identification of C15-C17 alkanes and alkenes in microalgal species suggests hydrocarbons may serve a similar function in a broad range of photosynthetic organisms.

Cyanobacteria (oxygenic photosynthetic bacteria) are found in nearly every environment on Earth and are major contributors to global carbon and nitrogen fixation (Galloway et al., 2004; Zwirgmaier et al., 2008). They are distinguished among prokaryotes in containing multiple internal thylakoid membranes, the site of photosynthesis, and a large protein compartment, the carboxysome, involved in carbon fixation. Despite these extra features, cyanobacteria can be as small as 0.6 μm in diameter (Raven, 1998).

All cyanobacteria with sequenced genomes encode the pathway for the biosynthesis of hydrocarbons, implying an important, although as-yet-undefined, role for these compounds (Lea-Smith et al., 2015). The major forms are C15-C19 alkanes and alkenes, which can be synthesized from fatty acyl-acyl-carrier proteins (ACPs) by one or other of two separate pathways (Fig. 1; Schirmer et al., 2010; Mendez-Perez et al., 2011). The majority of species produce alkanes and alkenes via

acyl-ACP reductase (FAR) and aldehyde deformylating oxygenase (FAD; Schirmer et al., 2010; Li et al., 2012; Coates et al., 2014; Lea-Smith et al., 2015). Cyanobacterial species lacking the FAR/FAD pathway synthesize alkenes via olefin synthase (Ols; Mendez-Perez et al., 2011; Coates et al., 2014; Lea-Smith et al., 2015). This suggests that hydrocarbons produced by either pathway serve a similar role in the cell. Homologs of FAR/FAD or Ols are not present in other bacteria or plant and algal species. However, C15-C17 alkanes and alkenes, synthesized by an alternate, uncharacterized pathway, were recently detected in a range of green microalgae, including *Chlamydomonas reinhardtii*, *Chlorella variabilis* NC64A, and several *Nannochloropsis* species (Sorigué et al., 2016). In *C. reinhardtii*, hydrocarbons were primarily localized to the chloroplast, which originated in evolution from a cyanobacterium that was engulfed by a host organism (Howe et al., 2008). Hydrocarbons may therefore have a similar role

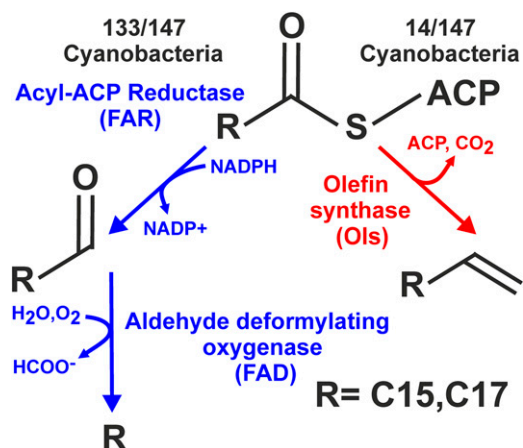


Figure 1. Hydrocarbon biosynthesis is encoded in all sequenced cyanobacteria. Detailed are the two hydrocarbon biosynthetic pathways, indicated in blue and red, respectively, in cyanobacteria. The number of species encoding the enzymes in each pathway is indicated.

in cyanobacteria, some green microalgae species, and possibly a broader range of photosynthetic organisms.

Hydrocarbons act as antidesiccants, waterproofing agents, and signaling molecules in insects (Howard and Blomquist, 2005) and prevent water loss, ensure pollen viability, and influence pathogen interactions in plants (Kosma et al., 2009; Bourdenx et al., 2011). However, the function of hydrocarbons in cyanobacteria has not been determined. Characterization of cyanobacterial hydrocarbon biosynthesis pathways has provided the basis for investigating synthetic microbial biofuel systems, which may be a renewable substitute for fossil fuels (Schirmer et al., 2010; Choi and Lee, 2013; Howard et al., 2013). However, secretion of long-chain hydrocarbons

from the cell into the medium, which is likely essential for commercially viable production, has not been observed in the absence of a membrane solubilization agent (Schirmer et al., 2010; Tan et al., 2011). Cyanobacterial hydrocarbons also have a significant environmental role. Due to the abundance of cyanobacteria in the environment, hydrocarbon production is considerable, with hundreds of millions of tons released into the ocean per annum following cell death (Lea-Smith et al., 2015). This production may be sufficient to sustain populations of hydrocarbon-degrading bacteria, which can then play an important role in consuming anthropogenic oil spills (Lea-Smith et al., 2015).

Here, we investigated the cellular location and role of hydrocarbons in both spherical *Synechocystis* sp. PCC 6803 (*Synechocystis*) and rod-shaped *Synechococcus* sp. PCC 7002 (*Synechococcus*) cells. We developed a model of the cyanobacterial membrane, which indicated that hydrocarbons aggregate in the middle of the lipid bilayer and, when present at levels observed in cells, lead to membrane swelling associated with pools of hydrocarbon. This suggested that alkanes may facilitate membrane curvature. In vivo measurements of *Synechococcus* thylakoid membrane conformation are consistent with this model.

RESULTS

Hydrocarbons Predominantly Localize to Thylakoid and Cytoplasmic Membranes

Recently we demonstrated that 115 sequenced cyanobacteria isolated from a broad range of environments contain either the *far/fad* or *ols* genes, encoding the enzymes for alkane/alkene biosynthesis (Lea-Smith et al., 2015). In an additional 32 recently sequenced genomes from cyanobacteria, we found the same situation with the majority, 133/147, containing *far/fad* homologs (Supplemental Table S1). Clearly, there is an important role for these compounds in cyanobacteria. In order to investigate this, we disrupted the two different biosynthetic pathways in two species of cyanobacteria that are also morphologically distinct. *Far* in *Synechocystis* and *ols* in *Synechococcus* were disrupted by insertion of a kanamycin resistance cassette into the open reading frame (Supplemental Fig. S1). In wild-type *Synechocystis*, 1.44 mg/g dry cell weight of alkanes, predominantly heptadecane and 8-heptadecene, were detected (Tan et al., 2011), whereas in *Synechococcus* 0.61 mg/g dry cell weight of alkenes, specifically nonadecene (Mendez-Perez et al., 2011), were present (Supplemental Fig. S2). In contrast, in mutant cells lacking either FAR or Ols, no hydrocarbons were observed. Complementation of Δ FAR by insertion of *far* into a neutral site on the chromosome restored alkanes to wild-type levels (Supplemental Figs. S1 and S2).

Due to their hydrophobic and nonpolar characteristics, hydrocarbons were expected to localize predominantly to membranes. This was confirmed in purified plasma and thylakoid membrane fractions from *Synechocystis* (Fig. 2, A and B). Alkanes constituted 5.63% and 17.41% of the

¹ T.L. was supported by Biotechnology and Biological Sciences Research Council (BBSRC) Research Grant BB/J016985/1 to C.W.M. D.J.L.-S. was supported by the Environmental Services Association Education Trust. L.L.B. was supported by a BBSRC Doctoral Training Grant (BB/F017464/1).

² Present address: Department of Life Sciences, Imperial College London, London SW7 2AZ, UK.

* Address correspondence to djl63@cam.ac.uk.

The author responsible for distribution of materials integral to the findings presented in this article in accordance with the policy described in the Instructions for Authors (www.plantphysiol.org) is: David J. Lea-Smith (djl63@cam.ac.uk).

D.J.L.-S. and C.J.H. conceived the original screening and research plans; D.J.L.-S., P.J.B., C.W.M., and C.J.H. supervised the experiments; D.J.L.-S., M.L.O.-S., T.L., D.J.N., L.L.B., M.P.D., L.P., R.G.H., C.A.R.C., G.M., P.B., and P.U. performed most of the experiments; D.J.L.-S., M.L.O.-S., T.L., D.J.N., L.L.B., M.P.D., R.G.H., T.J.S., P.J.B., C.W.M., and C.J.H. designed the experiments and analyzed the data; D.J.L.-S. conceived the project and wrote the article with contributions of all the authors; D.J.L.-S., P.J.B., C.W.M., and C.J.H. supervised and complemented the writing.

[OPEN] Articles can be viewed without a subscription.

www.plantphysiol.org/cgi/doi/10.1104/pp.16.01205

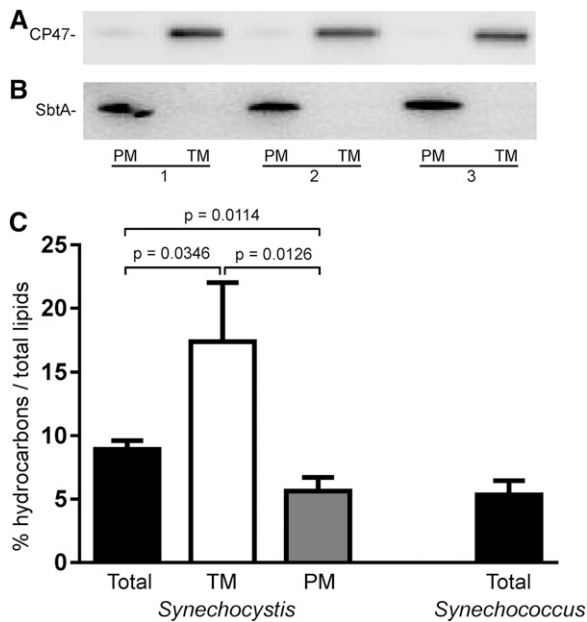


Figure 2. Hydrocarbons accumulate within cyanobacterial membranes. A and B, Detection of CP47 (A) and SbtA (B) in purified plasma and thylakoid membrane fractions (replicates 1–3). Small amounts of CP47 were consistently detected in the purified plasma membrane fractions. Five micrograms of protein was loaded with antibodies diluted 1:2000. PM, Plasma membrane; TM, thylakoid membrane. C, Percentage of hydrocarbons as total lipids in *Synechocystis* total, thylakoid and plasma membranes, and *Synechococcus* total membrane samples. Results are from three biological replicates. Mean \pm SD is indicated. Statistical significance was determined by a Student's *t* test.

plasma and thylakoid membrane lipid fractions, respectively (Fig. 2C; Supplemental Fig. S3). Alkanes comprised 8.92% of the total *Synechocystis* membrane lipid fraction. Given that thylakoids constitute a larger proportion of cellular membranes than plasma membranes, this suggests that a hydrocarbon-rich portion of the thylakoid membrane was purified during this process. In total *Synechococcus* membrane fractions, alkenes constituted 5.34% of total lipids (Fig. 2C).

Hydrocarbon-Deficient Strains Exhibit Enlarged Cell Size and Division Defects

To determine how loss of hydrocarbons affects cell morphology, we used bright-field microscopy. Δ FAR cells were significantly larger than wild-type *Synechocystis* (11.02 versus 4.63 μm^3 ; Fig. 3, A and B; Supplemental Fig. S4; Supplemental Table S2), which was confirmed via particle-counting measurements (11.49 versus 4.58 μm^3 ; Fig. 3C; Supplemental Table S3). In addition, a significantly larger percentage of Δ FAR cells were actively dividing (47.4% versus 40.1%; Fig. 3F; Supplemental Table S4). Division defects were also apparent in Δ Ols, which formed long chains of up to 12 cells and abnormal rods (Fig. 3D; Supplemental Fig. S4). The width of Δ Ols cells was significantly larger than wild-type *Synechococcus*

(1.76 versus 1.61 μm), which resulted in a significant increase in cell volume (3.89 versus 3.08 μm^3 ; Fig. 3E; Supplemental Table S2). Overall, these results indicate a role for hydrocarbons in limiting cell size and ensuring normal cell division.

Hydrocarbons Are Essential for Optimal Cell Growth

Strains were then cultured under continuous moderate light (40 $\mu\text{mol photons m}^{-2} \text{s}^{-1}$) to determine whether a lack of hydrocarbons in the membrane affected growth. Due to the difference in cell size between wild type and hydrocarbon-deficient mutants, which affects the optical properties of the culture (Fig. 4, A–D), growth was measured both by cell counting and by optical density. The increase in cell number during exponential growth was approximately 4-fold higher in wild-type *Synechocystis* cultures, compared to Δ FAR (Fig. 4A). Moreover, photobleaching increased in Δ FAR cells after 2 d growth, as measured by the amount of chlorophyll per cell (Fig. 4E). This suggests that cell damage was occurring during this time. The enlarged phenotype of Δ FAR was maintained over this growth period (Fig. 4G). Wild-type *Synechococcus* also demonstrated a statistically significant 1.4-fold increase in cell number during exponential growth compared to Δ Ols (Fig. 4B), although photobleaching was not observed (Fig. 4F). Under moderate light, when starting with an equal amount of culture as determined by optical density, growth of the wild type was 2.2-fold faster than Δ FAR (Supplemental Fig. S5A). Growth of wild-type *Synechococcus* was 1.5-fold faster than Δ Ols (Supplemental Fig. S5B). The difference in growth rates between wild-type *Synechocystis* and *Synechococcus* and the hydrocarbon-deficient mutants was similar at a higher light intensity of 120 $\mu\text{mol photons m}^{-2} \text{s}^{-1}$ (Supplemental Fig. S5, C and D). Overall, these results demonstrate the importance of hydrocarbons for optimal cell growth.

The Absence of Hydrocarbons Has Minor Effects on Photosynthetic Performance

Other cellular traits were then examined to determine whether these could affect cell growth. The maximum photosynthetic rate, as measured by oxygen evolution per unit of chlorophyll, was not reduced in the Δ FAR and Δ Ols mutants (Fig. 5, A and B). An increase in respiration was observed in Δ FAR cells, with a 2-fold higher rate observed compared to wild type (Fig. 5C). In algae, respiration increases with cellular size (Tang and Peters, 1995), and our data suggest that the same relationship may occur in cyanobacteria. Despite the increased respiratory rate, growth of Δ FAR was still impaired under light/dark cycles (Supplemental Fig. S6). However, respiration was similar between wild type and Δ Ols (Fig. 5D). Photoinhibition was also comparable between wild-type and hydrocarbon-deficient strains (Fig. 5, E and F).

The absorbance profile and emission spectra of the photosynthetic and light harvesting complexes were

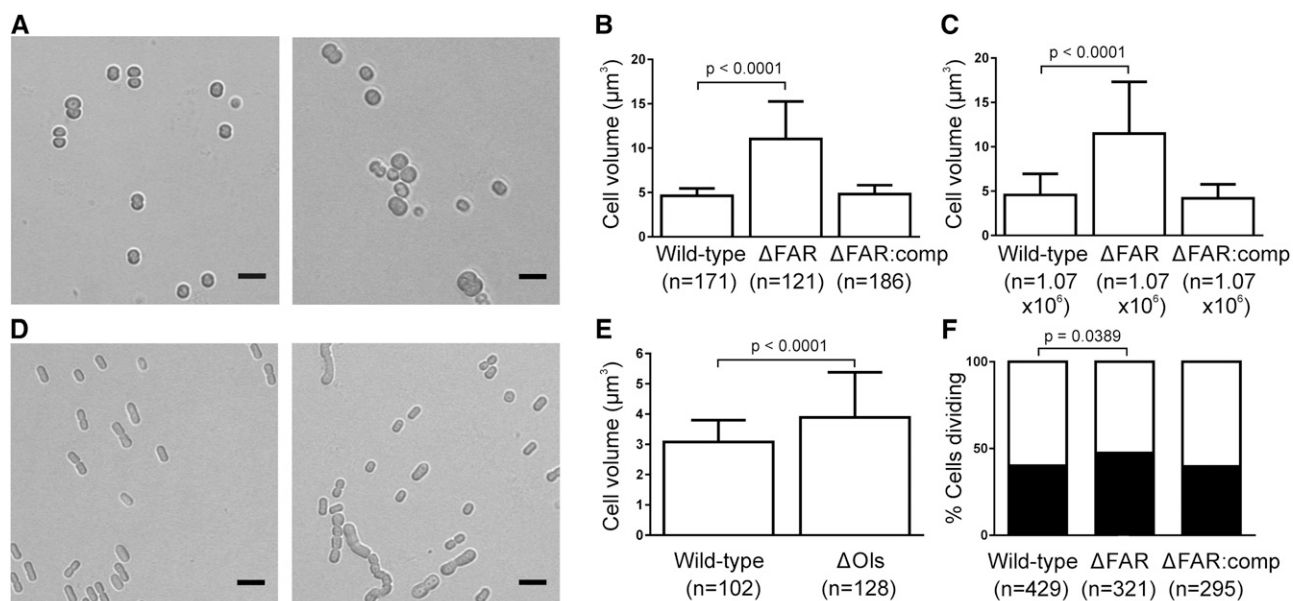


Figure 3. Hydrocarbon-deficient mutants have increased cell size and division defects. A, Bright-field images of wild-type *Synechocystis* (left) and Δ FAR (right) cells. Scale bars correspond to 5 μ m. B and C, Cell volume of *Synechocystis* strains quantified via measuring the diameter of cells from confocal microscopy images (B) and particle counting measurements (C). D, Bright-field images of wild-type *Synechococcus* (left) and Δ Ols (right) cells. Scale bars correspond to 5 μ m. E, Cell volume of *Synechococcus* strains quantified via measuring the width and length of cells from confocal microscopy images. B, C, and E, Mean \pm SD is indicated. Statistical significance was determined by a Student's *t* test. F, Percentage of single versus actively dividing *Synechocystis* cells. Statistical significance was determined by a two-way χ^2 test.

then examined. Absorbance was slightly reduced in both hydrocarbon-deficient mutants in the 400 to 550 nm range (Supplemental Fig. S7), the portion of the spectra corresponding to carotenoid and chlorophyll absorption. However, the carotenoid/chlorophyll ratio was not significantly different between strains (Supplemental Table S5), suggesting that the altered absorbance profile of the hydrocarbon-deficient mutants could be due to differences in light scattering, which have a greater effect at shorter wavelengths in the spectrum. Analysis of the hydrocarbon-deficient mutants via 77K fluorescence emission spectra showed minor but consistent differences in energy transfer efficiency from phycobilisomes to the reaction centers of photosystems in Δ FAR and Δ Ols, a blue shift in the peak between 680 and 700nm in Δ FAR, indicative of increased uncoupling of phycobilisomes from photosystems (Supplemental Fig. S8, A and B), and an altered photosystem II to photosystem I ratio (Supplemental Fig. S8, C and D). Given that the oxygen evolution rates of the hydrocarbon-deficient strains are similar to wild type, the cumulative effect of these changes on photosynthetic efficiency must be minor. Overall, these results suggest that differences in cell size and division may be the major factors in the impaired growth observed in hydrocarbon-deficient mutants.

Hydrocarbons May Induce Membrane Flexibility by Accumulating within the Lipid Bilayer

Molecular dynamics simulations have become an invaluable technique used to investigate the nanoscale

organization of lipid membranes (Marrink et al., 2009; Vattulainen and Rog, 2011), particularly in complex membrane systems (Ingólfsson et al., 2014; Manna et al., 2014). In order to understand how hydrocarbons could affect membrane properties, a novel symmetrical membrane model system was simulated based on the pseudoatomistic Martini force field, with an approximately 4:1 mapping of heavy atoms to coarse-grained particles (Supplemental Fig. S9; López et al., 2013). The present model used 16 different lipid types corresponding to the four major groups present in cyanobacteria: phosphatidylglycerol (PG), monogalactosyl-diacylglycerol (MGDG), digalactosyl-diacylglycerol (DGDG), and sulfoquinovosyl-diacylglycerol (SQDG), in a ratio as experimentally determined in *Synechocystis* (Supplemental Table S6; Sheng et al., 2011). The system contained a total of 2400 lipids, resulting in a large membrane slab with dimensions of approximately 21 \times 27 nm. The hydrocarbon heptadecane was added randomly to the solvent of the equilibrated membranes after 2 μ s and observed to enter the bilayer within the first 50 ps of simulation due to its hydrophobicity. Heptadecane became fully incorporated within \sim 20 ns, remained solvated within the membrane for the full 5 μ s of simulation, and was localized between the two monolayers, alongside the lipid tails at the center of the bilayer (Fig. 6, A–D).

In symmetrically modeled membranes where no flip-flopping of individual lipids across leaflets occurs, like the one studied here, a flat lamellar bilayer would be expected. This was the case in the absence of alkanes, in which a stable, noncurved membrane was observed

Figure 4. Hydrocarbons are essential for optimal growth of *Synechocystis* and *Synechococcus*. A to D, Growth of *Synechocystis* (A and C) and *Synechococcus* (B and D) under $40 \mu\text{mol photons m}^{-2} \text{s}^{-1}$ light. An equal number of cells, approximately 5×10^6 for *Synechocystis* strains and 1×10^7 for *Synechococcus* strains, was added to each culture. This corresponded to an $\text{OD}_{750\text{nm}}$ equal to 0.07 ± 0.001 , 0.127 ± 0.009 , and 0.06 ± 0.002 for wild-type *Synechocystis*, ΔFAR , and $\Delta\text{FAR:comp}$ (C), respectively, and 0.076 ± 0.003 and 0.105 ± 0.008 for wild-type *Synechococcus* and ΔOIs (D), respectively. The growth rate constants for wild-type *Synechocystis*, ΔFAR , and $\Delta\text{FAR:comp}$ were $1.24 \pm 0.20 \times 10^6$, $3.08 \pm 0.13 \times 10^5$ ($P = 0.0169$), and $1.52 \pm 0.14 \times 10^6$ cells h^{-1} , respectively, and for wild-type *Synechococcus* and ΔOIs were $1.98 \pm 0.02 \times 10^6$ and $1.42 \pm 0.04 \times 10^6$ cells h^{-1} ($P = 0.0009$), respectively. E and F, The amount of chlorophyll per cell (in attomol) in *Synechocystis* and *Synechococcus* strains, respectively. G, Cell diameter of *Synechocystis* strains. Results are from three biological replicates. Errors bars indicate SD. Asterisks indicate significant differences between wild-type and hydrocarbon-deficient samples (Student's paired t test: $P < 0.05$).

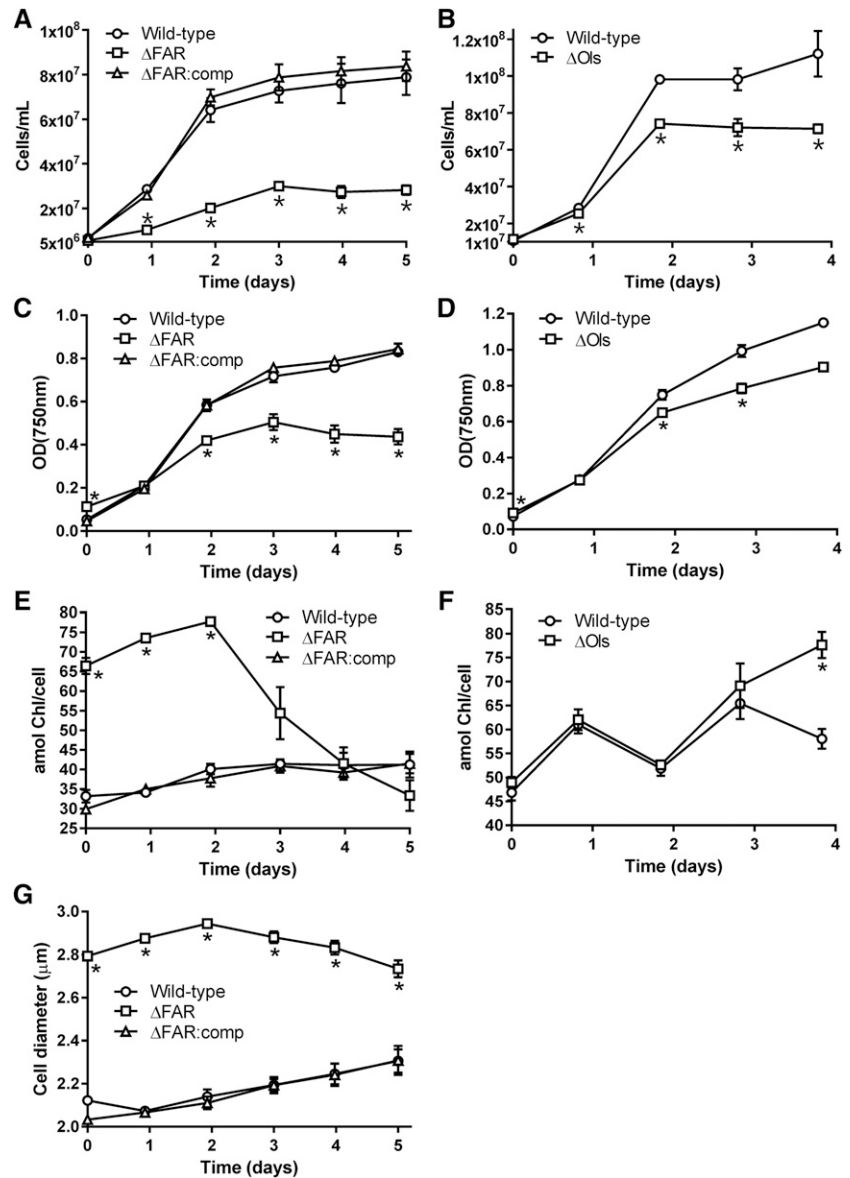


(Fig. 6A). Addition of hydrocarbons led to their spontaneous insertion and clustering within the bilayer core, with a concomitant increase in membrane thickness from ~ 3.27 nm to ~ 3.95 nm, irrespective of concentration. The overall lipid lateral diffusion coefficients in all systems were within experimentally reported ranges (Kařa, 2013). Pools of clustered hydrocarbon molecules were associated with a reduction in lipid chain order and packing efficiency, particularly at $\geq 5\%$ mol/mol hydrocarbon concentrations (Supplemental Fig. S10). Moreover, increasing amounts of hydrocarbon dissolved within the bilayer center, which led to localized swelling on one side of the membrane, around the sites of hydrocarbon accumulation, as visually evident in the cross sections (Fig. 6, B–D). The swelling settled in one direction or another, and this direction did not change during the simulation, presumably due to the stochastic

distribution of solubilized hydrocarbons within the membrane. This is consistent with neutron diffraction studies, which indicated alkane incorporation and swelling of dioleoyl lecithin bilayers (White et al., 1981). The accumulation of hydrocarbons thus increased the flexibility of the membrane and induced localized swelling. It should also be noted that the use of an alternative lipid parameter set developed for the membranes of *Thermosynechococcus vulcanus* and *Spinacia oleracea* (van Eerden et al., 2015) similarly induced swelling and disorder in our bilayer model in the presence of alkanes.

The level of swelling observed at $\geq 7.5\%$ mol/mol hydrocarbons due to the presence of a large hydrocarbon pool eventually destabilized the membrane, resulting in a phase transition to a nonlamellar bilayer. In a macroscopic system and/or under conditions of fixed simulation volume, the membrane swelling and

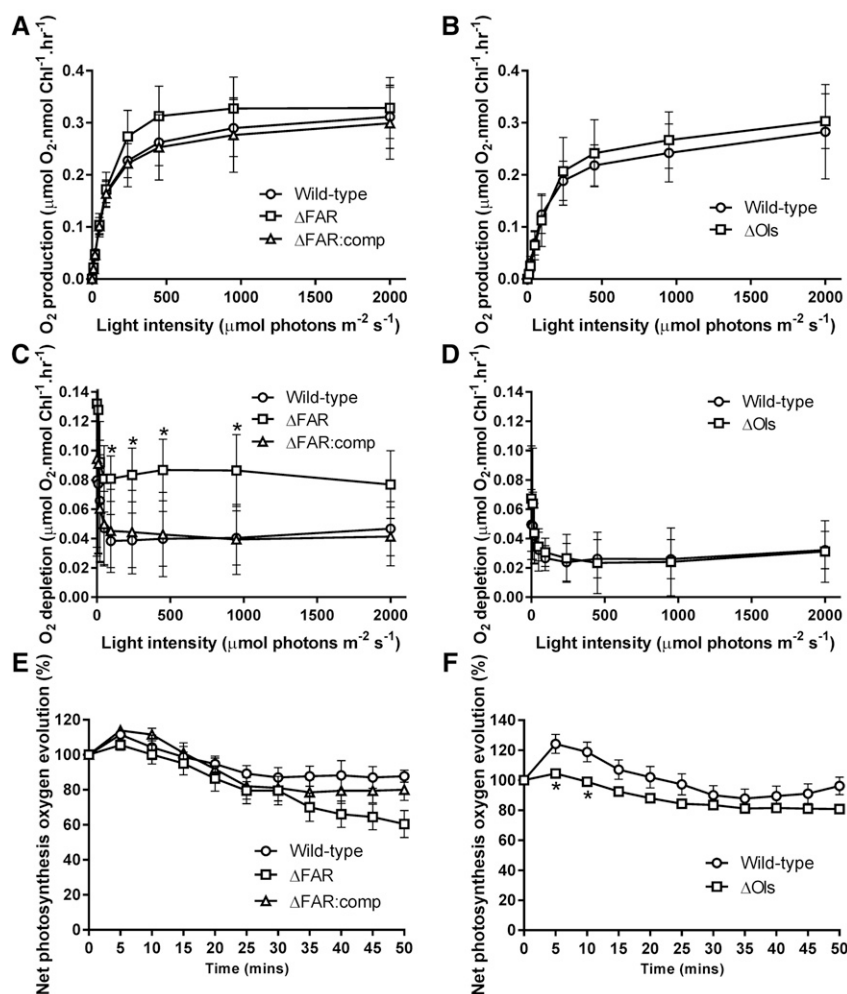


Figure 5. Photosynthetic rates and photoinhibition are similar between wild-type and hydrocarbon-deficient mutants. A and B, Oxygen evolution was measured at different light intensities in *Synechocystis* (A) and *Synechococcus* (B) to examine photosynthesis. The maximum photosynthetic rate of wild-type *Synechocystis*, ΔFAR, and ΔFAR:comp was 0.311 ± 0.025 , 0.329 ± 0.024 , and $0.299 \pm 0.028 \mu\text{mol O}_2 \text{ nmol Chl}^{-1} \text{ h}^{-1}$, respectively, and of wild-type *Synechococcus* and ΔOls was 0.283 ± 0.03 and $0.303 \pm 0.018 \mu\text{mol O}_2 \text{ nmol Chl}^{-1} \text{ h}^{-1}$, respectively. C and D, Respiration was determined by measuring oxygen consumption following each light period in *Synechocystis* (C) and *Synechococcus* (D). The average oxygen consumption rate following dark periods after $95 \mu\text{mol photons m}^{-2} \text{ s}^{-1}$ of wild-type *Synechocystis*, ΔFAR, and ΔFAR:comp was 0.041 ± 0.008 , 0.083 ± 0.006 , and $0.043 \pm 0.01 \mu\text{mol O}_2 \text{ nmol Chl}^{-1} \text{ h}^{-1}$, respectively, and of wild-type *Synechococcus* and ΔOls was 0.027 ± 0.005 and $0.027 \pm 0.007 \mu\text{mol O}_2 \text{ nmol Chl}^{-1} \text{ h}^{-1}$, respectively. E and F, Photoinhibition was determined by measuring oxygen evolution at a light intensity of $2000 \mu\text{mol photons m}^{-2} \text{ s}^{-1}$ in *Synechocystis* (E) and $3000 \mu\text{mol photons m}^{-2} \text{ s}^{-1}$ in *Synechococcus* (F). All results are from six to nine separate biological replicates. Error bars indicate sd. Asterisks indicate significant differences between wild-type and hydrocarbon-deficient samples (Student's paired *t* test: $P < 0.05$).

lipid disorder would be expected to result in induction of significant bilayer curvature. Typically, membrane curvature depends upon induced asymmetry of one monolayer compared to another (McMahon and Gallop, 2005). Local clustering of nonbilayer forming lipids could also lead to curvature. MGDG is one such lipid, whereas PG, DGDG, and SQDG favor flat lamellar phases (Shiple et al., 1973; Tilcock, 1986), and local MGDG enrichment could hinder the formation of complete lamellar bilayer phases, even in combination with other thylakoid lipids (Murphy, 1982).

Synechococcus Hydrocarbon-Deficient Mutants Demonstrate Reduced Membrane Curvature

To assess the effects of hydrocarbon deficiency on membrane conformation in *Synechocystis* and *Synechococcus*, we used thin-section electron microscopy. Electron micrographs of the wild-type and hydrocarbon-deficient mutants suggested that the thylakoid membranes are more planar in the mutants, although this effect could only be properly quantified and verified in *Synechococcus*, due to its more regular thylakoid membrane layout and its elongated cell

shape. In thin-section images from *Synechococcus*, we selected cells that appeared circular in profile: In these cases, we could be sure that the thin-section cut across the cell perpendicular to the long axis, since any other section would be noncircular (Supplemental Fig. S11). In the circular sections, the thylakoid membranes appear as an array of roughly parallel membrane sacs, each spanning the gap between a pair of poorly defined bodies close to the plasma membrane termed the "thylakoid centers" (Kunkel, 1982; Stengel et al., 2012). Typically, each thin section showed two to four thylakoid centers distributed around the cell perimeter, with the thylakoid membrane sacs extending between them.

To derive a quantitative measure of membrane curvature, we traced the membrane between two thylakoid centers and measured its length and also measured the straight-line distance between the thylakoid centers (Fig. 6E). The ratio of these two measures reflects the curvature of the membrane. We measured the curvature of over 100 membrane segments from each strain. There was no significant difference between the means of the wild type and ΔOls internode distances. On average, thylakoid membranes in wild-type cells were found to be more curved than those of ΔOls (Fig. 6F). The mean

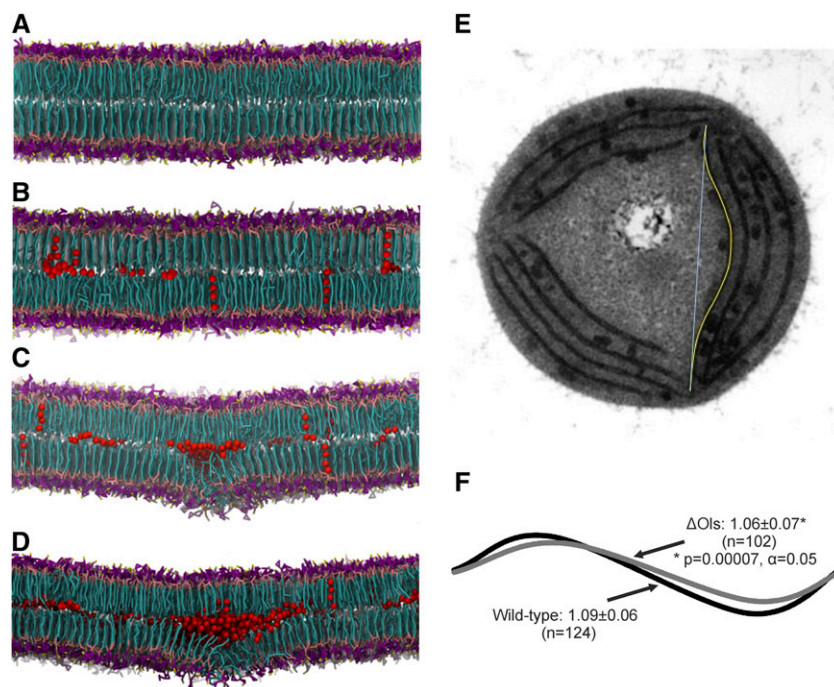


Figure 6. Hydrocarbons disrupt membrane order by integrating into the lipid bilayer. A to D, Modeling of cyanobacterial membranes containing (A) 0, (B) 2.5, (C) 5, and (D) 7.5 mol heptadecane/mol total lipids in the bilayer. Hydrocarbons are shown as red van der Waals spheres. Lipids are shown in stick representation and colored as follows: lipid head group rings in magenta, phosphate beads in tan, sulfate beads in yellow, diglycerol beads in pink, and lipid tails in cyan. Snapshots show the direction of swelling associated with alkane accumulation that the membranes settled into, which was stochastic. E, Electron micrograph of a transverse section of *Synechococcus*, illustrating measurement of the curvature index, given by the ratio of the length of the membrane section (yellow line) and the shortest distance between the ends of the membrane section (cyan line). F, Comparison of lines with curvature index derived from membrane measurements. Mean \pm SD is indicated. Statistical significance was determined by a two-tailed *t* test. The distance of the internode measurements was similar between strains (wild type: 616 ± 147 nm, Δ Ols: 582 ± 142 nm; two-tailed *t* test: $P = 0.1$, $\alpha = 0.05$).

length ratio was 1.09 ± 0.06 in wild type versus 1.06 ± 0.07 in Δ Ols, with the relatively high standard deviations reflecting a range of membrane curvatures in both the wild type and Δ Ols (Fig. 6F; Supplemental Fig. S12). Nevertheless, the difference in the means is highly significant, with a *P* value of 0.00007 from a Student's *t* test.

DISCUSSION

Here, we have shown a role for hydrocarbons in two morphologically different cyanobacterial species. While both hydrocarbon-deficient mutants display increased cell size, division defects, and reduced growth, a more severe phenotype was observed in Δ FAR cells (Figs. 3 and 4). Spherical cells have a larger fraction of highly curved membranes than rod-shaped cells. In the case of cyanobacteria, greater membrane flexibility would be required in order to incorporate multiple thylakoid membranes and to divide efficiently. High-resolution inelastic neutron scattering experiments of *Synechocystis* cells demonstrated dynamic flexibility within thylakoid membranes that differed between light and dark periods, suggesting that, if hydrocarbons

affect curvature, these compounds may also have a role in other cellular functions (Stingaciu et al., 2016). While the division dynamics of cyanobacteria are poorly understood, in the spherical bacterium *Staphylococcus aureus*, cells divide by first forming a septum, leading to development of two daughter cells connected via a narrow peripheral ring, followed by an abrupt separation event (Zhou et al., 2015). This form of division induces high stress on cellular components and is dependent on extreme curvature in membranes. A similar division event in *Synechocystis* and other spherical cyanobacteria requires the induction of membrane curvature not only in the cytoplasmic membrane but also in the thylakoid membranes, in order that these are efficiently distributed between daughter cells. By contrast, rod-shaped cells divide by first increasing in volume and length, followed by formation of a septum in the middle of the extended cell and subsequent separation (Wu and Errington, 2011). This form of cell division would require less induction of membrane curvature in the cytoplasmic membrane and thylakoid membranes and would be necessary at only one end of the cell. Interestingly, in the Δ Ols strain, hydrocarbons were more important for efficient daughter

cell separation than division, as shown by the formation of chains of cells (Fig. 3D).

Although the Δ Ols mutant showed significantly less thylakoid membrane curvature on average than wild-type *Synechococcus*, examples of membrane curvature could be observed in this strain (Fig. 6; Supplemental Fig. S11), despite the natural tendency of lipid bilayers to adopt a flat shape (Graham and Kozlov, 2010). Moreover, since simulations indicated that they integrate into the middle of the bilayer (Fig. 6, B–D), hydrocarbons would be unable to orient the direction of curvature, suggesting that their major role may be to induce the required flexibility in membranes. Therefore, hydrocarbons cannot be the only factor determining membrane curvature: Other factors must contribute to both the direction and maintenance of curvature. In addition it was observed that after successive rounds of subculturing, typically six to eight, that the size difference between the hydrocarbon-deficient mutants and wild-type strains was reduced and *Synechococcus* Δ Ols cells no longer formed chains of cells. That suggests that other factors in the cell were compensating for the loss of hydrocarbons.

An Arabidopsis (*Arabidopsis thaliana*) protein, CURT1A, has been shown to induce membrane curvature in chloroplast membranes (Armbruster et al., 2013). A homologous protein in *Synechocystis*, CurT, has recently been shown to have a similar role in thylakoid membranes (Heinz et al., 2016). Deletion of CurT resulted in a reduction in growth and extreme differences in thylakoid membrane organization, with the thylakoids appearing to cross the cytoplasm and not converging on the “thylakoid centers.” In contrast to Δ FAR, cell size was not affected, although photosynthesis was reduced. The Δ curT strain also displayed disassociated phycobilisomes, similar to what was observed in Δ FAR and Δ Ols (Supplemental Fig. S8, A and B). This strongly suggests that the degree of membrane curvature is essential for optimal phycobilisome:photosystem interaction and may also influence contact of other soluble proteins with membrane-bound components. Therefore, it is possible that, if hydrocarbons do alter membrane curvature, then this is augmented and orientated by CurT. In Δ curT, the thylakoid membranes were still highly curved, indicating that other factors are involved in inducing membrane curvature (Heinz et al., 2016). Homologs of CurT are present in the majority of sequenced cyanobacterial strains (Supplemental Table S1). Notable exceptions include *Gloeobacter* species, which lack thylakoid membranes (Rippka et al., 1974; Rexroth et al., 2011; Saw et al., 2013) and therefore may not require orientation of membrane curvature or may regulate it by other means. In other bacterial species, this includes turgor pressure or force applied via cytoskeletal components (Cabeen et al., 2009). The glycolipid MGDG may also help stabilize this curvature, given its tendency to favor nonlamellar phases (Shipley et al., 1973; Murphy, 1982; Tilcock, 1986). Other as-yet-unidentified factors may also contribute to membrane curvature.

Hydrocarbons may also have additional functions in cells not identified in this study, such as modulating membrane permeability (Valentine and Reddy, 2015). The use of planar lipid bilayers as model systems has demonstrated that the addition of hexadecane increases membrane thickness and reduces membrane permeability (Dilger and Benz, 1985). Therefore, the increase in cell size may be due to a combination of factors: differences in osmotic pressure due to reduced membrane permeability, outward physical pressure on the cell applied by a series of less-curved thylakoid membranes, and division impairment, which would result in hydrocarbon-deficient strains being larger than wild type before cell separation. However, in the case of *Synechococcus* cells, it is interesting that an increase in size was only observed along the long axis of the cell, where outward physical pressure applied by less-curved thylakoid membranes would be expected to have the greatest effect.

CONCLUSION

Given that maintaining optimal growth and cell division is important in all ecosystems (Raven, 1998), the role of hydrocarbons in supporting optimal growth through potentially inducing membrane flexibility and reducing membrane permeability may be sufficient to explain the strong evolutionary pressure to retain hydrocarbon biosynthesis in cyanobacteria. It may also explain why similar hydrocarbons are produced by some microalgae species. An additional advantage is that unlike phospholipids or proteins, hydrocarbons do not contain either phosphorus or nitrogen, which are limited in many environments, notably in the open ocean where *Synechococcus* and *Prochlorococcus* species dominate (Flombaum et al., 2013). Moreover, the nonreactive properties of hydrocarbons make them resistant to oxidative damage (Valentine and Reddy, 2015), which is a major issue in cyanobacteria due to constant electron production from photosynthesis and respiration (Lea-Smith et al., 2016a). Hydrocarbon-induced membrane curvature may therefore represent a unique, low-risk, and efficient system of inducing flexibility and reducing permeability in one of the most biologically important and ancient membrane systems on the planet.

MATERIALS AND METHODS

Bioinformatics

Protein BLAST comparisons (Altschul et al., 1990) were performed using inferred protein sequences for *Synechocystis* *sl10209* (FAR), *sl10208* (FAD), and *slr0483* (CurT) and *Synechococcus* *Syn7002_A1173* (Ols; WP_012306795) with the completed cyanobacterial genomes listed in the National Center for Biotechnology Information (NCBI) database (<http://www.ncbi.nlm.nih.gov/genome/browse/>) and Biller et al. (2014). For FASTA BLAST comparisons of Ols, only matches across the majority of the gene (>90%) were included, due to the conservation of many domains in polyketide synthase proteins. Protein BLAST comparisons of FAR, FAD, and Ols were also performed against the bacterial and eukaryotic sequences in the NCBI database in order to confirm that these proteins are cyanobacterial specific.

Bacterial Strains, Media, and Growth Conditions

Synechocystis and *Synechococcus* strains were routinely cultured in BG11 medium with 10 mM sodium bicarbonate (Castenholz, 1988) at 30°C and grown under moderate light (30–40 $\mu\text{mol photons m}^{-2} \text{s}^{-1}$) with shaking at 120 rpm unless otherwise indicated. HEPES and vitamin B12 were added to *Synechococcus* cultures to a final concentration of 10 mM and 4 $\mu\text{g/L}$, respectively. Ten millimolar sodium bicarbonate was also added to *Synechococcus* cultures every 2 d. Fifteen grams/liter of agar was used for preparation of solid media and supplemented with 30 to 100 $\mu\text{g/mL}$ of kanamycin or 5% Suc (w/v) when necessary. Cultures incubated at 120 $\mu\text{mol photons m}^{-2} \text{s}^{-1}$ were bubbled with air to prevent carbon limitation.

Plasmid Construction

All primers are listed in Supplemental Table S7. Polymerase chain reactions were performed by standard procedures using Phusion high-fidelity DNA polymerase (New England Biolabs). The genome sequence of *Synechocystis* and *Synechococcus* (Kaneko et al., 1996) was consulted via Cyanobase (<http://genome.kazusa.or.jp/cyanobase>) for primer design. Gene deletion of *Sll0209* was performed by amplifying a 1750-bp fragment spanning *Sll0209* and flanking regions using primers *Sll0209for* and *Sll0209rev*, followed by insertion into the *XbaI/SphI* sites of pUC19. The *aph* gene conferring kanamycin resistance was excised from pUC4K (Vieira and Messing, 1982) and inserted into the *HincII* site in the middle of the fragment to generate p*Sll0209*. Gene deletion of *ols* (SYNPPC7002_A1173) was performed by amplifying a 1922-bp fragment in the 5' region using primers *Olsfor* and *Olsrev*, followed by insertion into the *EcoRI/SalI* sites of pUC19. The *aph* gene was inserted into the blunt ended *BamHI* in the middle of the fragment to generate p*OLS*.

Gene deletion of *phaAB* was performed by amplifying a 1069-bp fragment upstream of *phaA* using primers *PhaABleftfor* and *PhaABleftrev* and a 1087-bp fragment downstream of *phaB* using primers *PhaABrightfor* and *PhaABrightrev*, followed by insertion of the respective fragments into the *XbaI/BamHI* and *SacI/EcoRI* sites of pUC19 to generate p*PhaAB-1*. The *BamHI*-digested *npt1/sacRB* cassette from pUM24Cm (Ried and Collmer, 1987) was inserted into the *BamHI* site between the upstream and downstream fragments to generate p*PhaAB-2*. To generate the plasmid for complementation (p*Sll0209comp*) of Δ *Sll0209*, the entire *Sll0209* gene plus 295 bp of upstream region and 263 bp of downstream region was amplified using primer pairs *Sll0209compfor* and *Sll0209comprev* and inserted into the *BamHI/SacI* sites of p*PhaAB-1*.

Generation of Mutant Strains

Generation of marked mutants was conducted according to Lea-Smith et al. (2013, 2016b). Approximately 1 μg of plasmids p*Sll0209*, p*OLS*, and p*PhaAB-2* was mixed with *Synechocystis* or *Synechococcus* cells for 6 h in liquid medium, followed by incubation on BG11 agar plates for approximately 24 h. An additional 3 mL of agar containing kanamycin was added to the surface of the plate followed by further incubation for approximately 1 to 2 weeks. Transformants were subcultured to allow segregation of mutant alleles. In the case of the hydrocarbon-deficient mutants, this was performed by streaking the strains on BG11 agar plates containing 30 $\mu\text{g/mL}$ of kanamycin, followed by a subsequent restreak on a BG11 agar plate containing 100 $\mu\text{g/mL}$ of kanamycin. Typically, segregated mutants were obtained within 2 weeks. This is in contrast to a recent report, in which hydrocarbon-deficient *Synechocystis* mutants were only obtained after approximately 6 months, most likely due to these strains being segregated on BG11 agar plates containing a maximum of 40 $\mu\text{g/mL}$ of kanamycin (Berla et al., 2015). Repeated streaking over a 6-month period could also result in selection of numerous secondary mutations. Given that a complemented strain was not generated or examined in the Berla et al. (2015) study, it is therefore impossible to determine whether the phenotype observed was caused by deletion of hydrocarbons or secondary mutations. Due to this factor and the difference in time in generating mutants, a direct comparison between the results reported by Berla et al. (2015) and this study is difficult due to the instability of the hydrocarbon-deficient strains.

Segregation was confirmed by PCR using primers *Sll0209for/Sll0209rev*, *Olsfor/Olsrev*, or *Phafor/Pharev*, which flank the inserted region (Supplemental Fig. S1). Generation of unmarked mutants was carried out according to Xu et al. (2004) and Lea-Smith et al. (2013, 2016b). To remove the *npt1/sacRB* cassette and insert the *Sll0209* complementation cassette, the *phaAB*-marked knockout was transformed with 1 μg of the markerless p*Sll0209comp* construct. Following incubation in BG11 liquid medium for 4 d and agar plates containing Suc for a

further 1 to 2 weeks, transformants were patched on kanamycin and Suc plates. Suc-resistant, kanamycin-sensitive strains containing the unmarked deletion were confirmed by PCR using primers flanking the insert region (Supplemental Fig. S1B). The Δ *Sll0209* mutant was generated in the Δ *PhaAB:Sll0209* background in order to produce the complement strain.

The Δ *OLS* mutant could not be complemented due to the large size of the gene (8163 bp). Therefore, wild-type *Synechococcus* and Δ *OLS* were sequenced using the Illumina MiSeq personal sequencer and mapped to the *Synechococcus* genome. Apart from the expected deletion in *ols*, only a single point mutation in Δ *OLS*, leading to a silent mutation, was observed when compared to the wild type.

For characterization, mutant strains were subcultured in liquid medium no more than two times and streaked on solid medium a maximum of six times, due to the instability of the mutants. After this period, the size difference between the hydrocarbon-deficient mutants and wild-type strains was reduced, suggesting that another factor in the cell was compensating for the loss of hydrocarbons. Strains could not be prepared as glycerol stocks, since this also resulted in a change in the phenotype. After this period of subculturing, fresh mutants were constructed for analysis.

Extraction and Analysis of Total Hydrocarbons

All chemicals were purchased from Sigma chemicals. For extraction of total hydrocarbons, 1.5 mL of dichloromethane was added to pelleted dried cells in glass vials, and hydrocarbons were extracted and analyzed by gas chromatography-mass spectrometry (GC-MS) according to Lea-Smith et al. (2015). Hydrocarbons and lipids were extracted from *Synechocystis* thylakoid, cytoplasmic, and total membrane fractions, and *Synechococcus* total membrane fractions based on the method in Davey et al. (2008) where 1 mL (3 mL for total membrane fractions) of chilled (-20°C) solvent (methanol:chloroform:water, 2.5:1:1) was added to the membrane fraction tube, vortexed, and left in ice with occasional shaking. After 30 min, tubes were centrifuged (16,000g, 2 min, 4°C). The supernatant was removed and placed in a chilled tube on ice. The remaining pellet was re-extracted with 0.5 mL (1.5 mL for total membrane fractions) chilled (-20°C) methanol:chloroform 1:1 for 30 min. After centrifuging as described previously, the supernatants were combined in a 2 mL tube. The organic chloroform phase was separated from the aqueous phase by adding 250 μL (750 μL) chilled water and extracted into a new glass 2 mL GC sample vial. The chloroform phase was dried (GeneVac EZ-2; SP Scientific) and resuspended in 200 μL heptane. The extracts were stored at -80°C before analysis of total alkanes and lipids (fatty acid methyl esters [FAMES]). For negative controls, extraction blanks were carried out without cyanobacteria (no significant amounts of hydrocarbons were detected) and positive controls consisted of adding 1 mg/mL standard alkane mix (Sigma C8-C20 alkane mix) to a blank extraction procedure.

Purification of Membrane Fractions

Plasma and thylakoid membranes were isolated using a combination of Suc density centrifugation followed by aqueous two-phase partitioning according to Norling et al. (1998) and Huang et al. (2002). *Synechocystis* cells were grown at 30°C under 50 $\mu\text{mol photons m}^{-2} \text{s}^{-1}$ of white light in BG11 medium with bubbling air. All steps were carried out at 4°C unless otherwise stated. Two liters of cells harvested at $\text{OD}_{750\text{nm}} = 0.9$ to 1.0 were resuspended in buffer A (20 mM potassium phosphate, pH 7.8) and broken with glass beads. Unbroken cells and debris was pelleted by centrifugation at 3000g for 10 min. The supernatant was centrifuged at 103,000g for 30 min to pellet total membranes. Total membranes were made up to a concentration of 42% Suc by the addition of solid Suc and placed onto a discontinuous Suc gradient comprising of 3 mL layers of 50% (w/w), 42% (w/w with total membranes), 40% (w/w), 38% (w/w), 35% (w/w), 30% (w/w), and 10% (w/w) Suc in buffer A and centrifuged at 125,000g for 15 h. The fraction between 38% and 42% was collected, diluted with buffer A, and centrifuged at 125,000g for 45 min to pellet membranes. Pelleted membranes were homogenized in buffer B (5 mM potassium phosphate, pH 7.8, 0.25 M Suc) to a weight of 3.75 g and applied to a 6.25 g polymer mixture of 5.8% Dextran T-500 and 5.8% polyethylene glycol 3350 in buffer B. The partitioning system was gently inverted 35 times at 4°C and centrifuged at 1000g to facilitate phase separation. Pure thylakoid membranes were obtained from the lower phase after five further partitionings in the 5.8% polymer mixture. Pure plasma membranes were obtained from the ninth upper phase after three partitionings in the initial polymer mixture of 5.8%, three further partitionings in 6.2%, and a final three partitionings in 6.4%. Purified plasma and thylakoid membranes were

diluted in buffer B and pelleted by centrifugation at 125,000g for 1 h and homogenized in a minimal volume of the same buffer.

Identification and Quantification of Hydrocarbons in the Membrane Fractions

Hydrocarbons in the heptane extract were identified by GC-MS (Thermo Scientific Trace GC 1310-ISQ LT Single Quadrupole EI MS, A1-1310 Autosampler) with a Phenomenex Zebtron ZB-5MSi Capillary GC Column (30 m × 0.25 mm × 0.25 μm). The injection volume was 1 μL with a 10:1 split ratio with an injector temperature of 300°C, using helium as a carrier gas at a constant flow of 1.0 mL min⁻¹. The following gradient was used: initial oven temperature 70°C, 2 min; 76°C, 1 min; 250°C at 6°C min⁻¹; and 330°C at 50°C min⁻¹. The transfer line temperature was 250°C. The mass spectrometry conditions in the positive mode were ion source, 250°C; mass range 45 to 650 D; and scan time of 0.35 s. Heptadecane and nonadecene were identified by coretentation with standards and NIST mass spectral search libraries (National Institute of Standards and Technology NIST v2.0); 8-heptadecene was identified using the NIST library alone. Heptadecane and nonadecene were quantified using standard curves derived from peak areas of heptadecane and nonadecene standards; 8-heptadecene was quantified using peak areas derived from heptadecane standards (0.06–31 μg/mL).

Identification and Quantification of Total Lipids in the Membrane Fractions

The total lipid content of the heptane extract was converted to FAMES as described by Davey et al. (2014). The FAMES were separated and identified using GC-MS as described in the membrane alkane analysis section but with a 35:1 split injection ratio, injector temperature of 230°C, helium at a constant flow rate of 1.2 mL min⁻¹, and with the following gradient: initial oven temperature, 60°C for 2 min; 150°C at 15°C min⁻¹; and 230°C at 3.4°C min⁻¹. The detector temperature was 250°C with a scan time of 0.174 s. FAMES were identified by coelution with a FAME standards and NIST libraries and were quantified and summed using standard curves derived from C16:0 methyl esters.

Modeling of *Synechocystis* Membranes

The *in silico* cyanobacterial membrane lipid compositions were based on the experimental lipid extractions and characterization of *Synechocystis* by Sheng et al. (2011). Four major classes of cyanobacterial lipids were used: PG, MGDG, DGDG, and SQDG, with various acyl tails differing in length and degree of saturation. These lipids contain a palmitic (16:1^{Δ9}) tail at the *sn*-2 position and another acyl tail of variable length and saturation at the *sn*-1 position (Murata et al., 1992). The composition of the lipid tails in the *in silico* membranes was adapted to coarse-grained resolution, i.e. an approximately 4:1 mapping of heavy atoms to coarse-grained particles, using the Martini force field (López et al., 2013). The structure of the lipid head groups and representative tails included in the model are compared to their coarse-grained topologies in Supplemental Figure S9, where the mapping of the Martini bead types are shown and labeled. Standard bonded parameters were used. The compositions determined by Sheng et al. (2011) are shown in Supplemental Table S6, and compared to the number of lipids used in our model membranes to reproduce as closely as possible this composition. The hydrocarbon heptadecane was added in varying quantities to study the effects of this compound on membrane properties.

A total of 2400 lipids were used to build symmetric bilayers, consisting of 16 different lipid types. The system was solvated with 11,323 water beads, corresponding to ~45,000 waters, ensuring that the bilayer was well hydrated. Hydrated sodium counterion particles were added to neutralize the charges of PG and SQDG lipids. Heptadecane was added randomly to the solvent in the equilibrated membranes after 2 μs. The amounts used were 2.5, 5.0, and 7.5 mol %, corresponding to 60, 120, and 180 alkane molecules, respectively. The initial unit cell dimensions of all membrane systems were 21.0 × 27.5 × 9.0 nm in the *x*, *y*, and *z* directions.

Simulation Details

The molecular dynamics simulations were performed using the GROMACS 4.5.5 MD package. The Martini lipid force field was used (Marrink et al., 2007) due to its proven performance in describing complex lipid membrane

properties. Initially, a system containing 200 randomly placed 18:1 DGDG molecules surrounded by solvent was simulated for 200 ns, yielding a pre-equilibrated bilayer. The lipid types were then converted at random to yield a membrane with the appropriate composition (Supplemental Table S6), using in-house code. Following minimization and a further 200 ns equilibration, the coordinates of this bilayer system were then multiplied in the *x*- and *y*-dimensions to produce the full 2400 lipid bilayer. A 1 μs equilibration simulation followed. Steepest descent was used for minimization, and a 40 fs time step was used together with the leap-frog algorithm during simulations. Lennard-Jones (excluding scaled 1–4) interactions were smoothly switched off between 0.9 and 1.2 nm using a force switch. Electrostatic interactions were calculated using a shifted potential with a cutoff of 1.2 nm, with a distance-dependent dielectric constant of 15. The neighbor list of 1.4 nm was updated every 10 steps. The isothermal-isobaric ensemble was used. The pressure (1 bar) and temperature (316 K) coupling parameters were set to 5 ps semi-isotropically, and 10 ps, respectively (Berendsen et al., 1984). All systems were simulated for 5 μs.

Electron Microscopy

Synechococcus cultures were grown to OD_{750nm} = ~0.3 and harvested by centrifugation (3000g; 10 min), fixed, and embedded according to the protocol described in Nürnberg et al. (2014) using potassium permanganate as additional fixative. Thin sections were cut with a glass knife at a Reichert Ultracut E microtome and collected on uncoated, 300 mesh copper grids. High contrast was obtained by poststaining with saturated aqueous uranyl acetate and lead citrate (Reynolds, 1963) for 4 min each. The grids were examined in a JOEL JEM-1230 transmission electron microscope at an accelerating potential of 80 kV.

Curvature Measurements

In transverse sections, the thylakoid membranes, three to five membranes thick, of wild-type *Synechococcus* and ΔOIs cells appear to emanate from three to four well-spaced nodes on the edge of the cell, like pages that fan out from the spine of a book that is lying open. The “spine” of this “book” can be imagined to run longitudinally along the cell from pole to pole. Spline curves were hand-fitted to individual membrane layers as far as they could be traced by eye from node to node in ImageJ. The ratio of the length of the curved line drawn to its Feret diameter (maximum caliper distance, i.e. the straight line distance between start and end points of the line in most cases) was taken to be a measure of its curvature. The 124 membranes from nine wild-type cells and 102 membranes from 12 ΔOIs cells were analyzed. Statistical tests were performed in Matlab.

Confocal Fluorescence Microscopy

For confocal microscopy, midlogarithmic phase cells were spotted onto BG11 1% (w/v) agar plates and visualized with a Leica laser-scanning confocal microscope SP5 using a ×63 oil-immersion objective (Leica HCX PL APO lambda blue 63.0×1.40 OIL UV). Chlorophyll *a* fluorescence was detected by using an excitation wavelength of 488 nm and an emission range from 670 to 720 nm. Images were captured with a pinhole of 95.5 μm, which corresponds to an optical section thickness of 0.8 μm and by 4× line averaging. Analyses were performed with ImageJ 1.47i (<http://imagej.nih.gov/ij>) and Origin. The cell volume was determined from the mean diameter for *Synechocystis* cells assuming a sphere, and from the mean diameter and width of *Synechococcus* cells by assuming an ellipsoidal shape. A Student's *t* test was used for comparison of cell volumes between strains with *P* < 0.05 being considered statistically significant.

Cell Counting

Numbers of cells per unit of volume were measured by counting the cells directly using a Beckman Coulter Z2 particle counter. Measurements were performed by diluting 20 to 100 μL of cells in 10 mL of measuring buffer. The cell diameter of *Synechocystis* cells was directly measured using the same instrument. Cell volume was calculated from these measurements. Due to the rod shape of *Synechococcus*, the cell size of this bacterium could not be determined using this device.

Cell Division

A semiautomated counting of cells was used to determine the number of cells that were in the process of division by segmenting the image based on

fluorescence intensity and cell size. A frequency table of the number of cells observed to be above and below the size threshold (interpreted to be dividing and divided, respectively) was generated (Supplemental Table S4). A two-way χ^2 test yielded a significant result, showing that the proportions of dividing versus divided cells is not independent of the strain and therefore suggests that there are more dividing cells in Δ FAR than in the wild type with statistical significance.

Measurements of Cell Growth

Growth rate constants as determined by cell counting were calculated during early exponential phase (0–46 h and 0–44 h, respectively, for *Synechocystis* and *Synechococcus* strains cultured under 40 μ mol photons $m^{-2} s^{-1}$ light). Growth rate constants as determined by optical density were calculated during early exponential phase (0–40 h and 0–90 h, respectively, for *Synechocystis* strains cultured under 40 and 120 μ mol photons $m^{-2} s^{-1}$ light; 0–26 h and 0–90 h, respectively, for *Synechococcus* strains cultured under 40 and 120 μ mol photons $m^{-2} s^{-1}$ light; and 18–78 h for *Synechocystis* strains cultured under 12 h light [40 μ mol photons $m^{-2} s^{-1}$ /12 h dark cycles]). A Student's paired *t* test was used for comparison of growth between strains, $P < 0.05$ being considered statistically significant.

Chlorophyll Measurements

The amount of chlorophyll in *Synechocystis* samples was measured by subtracting the 750 nm optical density (OD) value from the 680 nm OD value and multiplying the total by 10.854, according to Lea-Smith et al. (2013). To determine the correlation between OD values versus the chlorophyll concentration of *Synechococcus*, a range of samples was measured at 750 nm and 680 nm, in addition to measuring the chlorophyll concentration according to the method of Porra et al. (1989). A strong correlation ($r^2 = 0.9983$) was observed (Supplemental Fig. S13). The amount of chlorophyll in *Synechococcus* samples was then measured by subtracting the 750 nm OD value from the 680 nm OD value and multiplying the total by 12.959.

Photosynthesis, Photoinhibition, and Respiration Measurements

Photoinhibition, photosynthesis, and respiration were determined according to Lea-Smith et al. (2014). Photosynthetic O_2 evolution rates and O_2 depletion rates (respiration) were determined on cell cultures at $OD_{750nm} = \sim 0.5$ (~ 2.3 nmol Chl ml^{-1} in *Synechocystis* or ~ 4 nmol Chl ml^{-1} in *Synechococcus*) using an oxygen electrode system (Hansatech) maintained at 30°C. Δ FAR cell cultures were collected at an $OD_{750nm} = \sim 0.4$ and concentrated to an $OD_{750nm} = \sim 0.5$ prior to analysis. Following dark equilibration (10 min), O_2 exchange rates were recorded for 10 min at increasing light intensities (10, 20, 50, 95, 240, 450, 950, and 2000 μ mol photons $m^{-2} s^{-1}$), using Realite MR16+C 24°, 12 V, 50 W C13 white LED lamps (Deltech), which have a spectra similar to sunlight. Each light period was followed immediately by 10 min in darkness to calculate the respiration rates. The respiration rate following illumination at each light intensity period was subtracted to estimate the real rate of photosynthetic O_2 evolution. To measure photoinhibition, cell cultures of $OD_{750nm} = \sim 0.2$ (~ 1 nmol Chl ml^{-1} in *Synechocystis* or ~ 1.3 nmol Chl ml^{-1} in *Synechococcus*) were first dark equilibrated (10 min), and the rate of O_2 evolution was recorded for 50 min at a light intensity of 2000 μ mol photons $m^{-2} s^{-1}$ in *Synechocystis* and 3000 μ mol photons $m^{-2} s^{-1}$ in *Synechococcus*. All measurements were standardized to the initial rate. A Student's paired *t* test was used for all comparisons, $P < 0.05$ being considered statistically significant.

77 K Fluorescence

We performed 77 K fluorescence measurements on cells harvested during the exponential growth phase at an $OD_{750nm} = \sim 0.3$, diluted to a final chlorophyll concentration of 5 μ M and placed into glass sample tubes. After dark adaptation at room temperature for approximately 10 min, samples were then snap-frozen in liquid nitrogen. We recorded 77 K fluorescence emission spectra by a Perkin Elmer LS55 fluorescence spectrometer from 620 to 800 nm with either 600 nm (phycobilisome excitation) or 435 nm (chlorophyll excitation).

Absorbance Measurements

Absorbance measurements on whole cells were performed according to Lea-Smith et al. (2014). Cultures were harvested during the exponential

growth phase at an $OD_{750nm} = \sim 0.4$. Cultures were placed in a 4 mL fluorescence cuvette (1 cm path length) and positioned in front of the entrance port of an integrating sphere. A light source sent light via an input fiber into the cuvette containing the sample and the light leaving the sample in the forward direction was collected by the integrating sphere. The extinction spectra were recorded using a USB4000-UV-VIS Ocean Optics spectrometer connected to the integrating sphere with an output fiber optic and interfaced to a computer. The cuvettes containing the samples were positioned at different distances (0 mm and 5 mm) from the entrance port of the sphere, and the absorbance spectrum was obtained via the SpectraSuite Spectroscopy operating software. The nominal absorption spectrum was then calculated using the equation according to Merzlyak and Naqvi (2000).

Carotenoid Quantification

HPLC was performed to analyze carotenoid/chlorophyll *a* ratios. Pigments were extracted from freeze-dried samples (triplicates) by three subsequent extraction steps in ice-cold methanol. After addition of methanol, the samples were vortexed vigorously, incubated on ice for 10 min, and centrifuged for 10 min at 4°C at 14,000 rpm. The supernatants of all three extraction steps were combined and filtered using 13 mm, 0.22 μ m PTFE syringe disc filters. Two hundred microliters of each sample was loaded onto a Dionex HPLC system, which was equipped with a LiChrospher 100 RP-18 (5 μ m) reverse-phase column (Merck 1.50943.0001). The flow rate was set at 1 mL/min and the mobile phase composed of two eluents (A, 0–12 min; B, 12–23 min; A: 87% acetonitrile, 10% methanol, 3% 0.1 M Tris buffer pH 8; B: 80% methanol, 20% hexane). Pigments were detected spectrophotometrically at 447 nm, and absorbance spectra data were collected from 350 to 750 nm. The relative quantity of each pigment resolved was determined by integration of the area under the 447 nm peak (mAU \times min). Pigments were identified using published absorbance spectra data (Mohamed and Vermaas, 2004).

Supplemental Data

The following supplemental materials are available.

Supplemental Figure S1. Generation of mutant strains in *Synechocystis* and *Synechococcus*.

Supplemental Figure S2. Chromatograms showing separation of hydrocarbons from whole cells.

Supplemental Figure S3. Chromatograms showing separation of hydrocarbons from membrane fractions.

Supplemental Figure S4. Bright-field confocal images of *Synechocystis* and *Synechococcus* strains.

Supplemental Figure S5. Growth of *Synechocystis* and *Synechococcus* under moderate and high light.

Supplemental Figure S6. Growth of *Synechocystis* under moderate light/dark cycles.

Supplemental Figure S7. Absorbance profiles of *Synechocystis* and *Synechococcus* strains.

Supplemental Figure S8. 77K fluorescence of *Synechocystis* and *Synechococcus* strains.

Supplemental Figure S9. CG topologies of representative lipids of the membrane.

Supplemental Figure S10. Membrane partial density, lipid acyl chain order parameter, and organization in differing hydrocarbon contents.

Supplemental Figure S11. Electron microscopy images of *Synechococcus* cells.

Supplemental Figure S12. Length ratios (curvatures) of membranes from *Synechococcus* 7002 strains.

Supplemental Figure S13. Correlation between the absorbance at 680 nm and 750 nm, and amounts of chlorophyll measured following methanol extraction.

Supplemental Table S1. Conservation of hydrocarbon biosynthetic pathway proteins and CurT in sequenced cyanobacteria strains.

- Supplemental Table S2.** Cell size as determined via fluorescence microscopy.
- Supplemental Table S3.** Cell size as determined via particle counting measurements.
- Supplemental Table S4.** Cell counts of single and actively dividing *Synechocystis* cells.
- Supplemental Table S5.** Carotenoid/chlorophyll ratios in cyanobacterial strains.
- Supplemental Table S6.** Lipid composition of cyanobacterial membranes.
- Supplemental Table S7.** Sequence of primers used in this study.

ACKNOWLEDGMENTS

We thank Pietro Cicuta (Department of Physics, University of Cambridge), Gabriele Kaminski Schierle (Department of Chemical Engineering and Biotechnology, University of Cambridge) and James Locke, Arijit Das, and Bruno Martins (Sainsbury Laboratory, Cambridge) for useful discussion.

Received August 1, 2016; accepted October 3, 2016; published October 5, 2016.

LITERATURE CITED

- Altschul SF, Gish W, Miller W, Myers EW, Lipman DJ (1990) Basic local alignment search tool. *J Mol Biol* **215**: 403–410
- Armbruster U, Labs M, Pribil M, Viola S, Xu W, Scharfenberg M, Hertle AP, Rojahn U, Jensen PE, Rappaport F, et al (2013) *Arabidopsis* CURVATURE THYLAKOID1 proteins modify thylakoid architecture by inducing membrane curvature. *Plant Cell* **25**: 2661–2678
- Berendsen HJC, Postma JPM, van Gunsteren WF, Dinola A, Haak JR (1984) Molecular dynamics with coupling to an external bath. *J Chem Phys* **81**: 3684–3690
- Berla BM, Saha R, Maranas CD, Pakrasi HB (2015) Cyanobacterial alkanes modulate photosynthetic cyclic electron flow to assist growth under cold stress. *Sci Rep* **5**: 14894
- Biller SJ, Berube PM, Berta-Thompson JW, Kelly L, Roggensack SE, Awad L, Roache-Johnson KH, Ding H, Giovannoni SJ, Rocap G, et al (2014) Genomes of diverse isolates of the marine cyanobacterium *Prochlorococcus*. *Sci Data* **1**: 140034
- Bourdenx B, Bernard A, Domergue F, Pascal S, Léger A, Roby D, Pervent M, Vile D, Haslam RP, Napier JA, et al (2011) Overexpression of *Arabidopsis* ECERIFERUM1 promotes wax very-long-chain alkane biosynthesis and influences plant response to biotic and abiotic stresses. *Plant Physiol* **156**: 29–45
- Cabeen MT, Charbon G, Vollmer W, Born P, Ausmees N, Weibel DB, Jacobs-Wagner C (2009) Bacterial cell curvature through mechanical control of cell growth. *EMBO J* **28**: 1208–1219
- Castenholz RW (1988) Culturing methods for cyanobacteria. *Methods Enzymol* **167**: 68–93
- Choi YJ, Lee SY (2013) Microbial production of short-chain alkanes. *Nature* **502**: 571–574
- Coates RC, Podell S, Korobeynikov A, Lapidus A, Pevzner P, Sherman DH, Allen EE, Gerwick L, Gerwick WH (2014) Characterization of cyanobacterial hydrocarbon composition and distribution of biosynthetic pathways. *PLoS One* **9**: e85140
- Davey MP, Burrell MM, Woodward FI, Quick WP (2008) Population-specific metabolic phenotypes of *Arabidopsis lyrata* ssp. *petraea*. *New Phytol* **177**: 380–388
- Davey MP, Horst I, Duong GH, Tomsett EV, Litvinenko ACP, Howe CJ, Smith AG (2014) Triacylglyceride production and autophagous responses in *Chlamydomonas reinhardtii* depend on resource allocation and carbon source. *Eukaryot Cell* **13**: 392–400
- Dilger JP, Benz R (1985) Optical and electrical properties of thin monolein lipid bilayers. *J Membr Biol* **85**: 181–189
- Flombaum P, Gallegos JL, Gordillo RA, Rincón J, Zabala LL, Jiao N, Karl DM, Li WK, Lomas MW, Veneziano D, et al (2013) Present and future global distributions of the marine Cyanobacteria *Prochlorococcus* and *Synechococcus*. *Proc Natl Acad Sci USA* **110**: 9824–9829
- Galloway JN, Dentener FJ, Capone DG, Boyer EW, Howarth RW, Seitzinger SP, Asner GP, Cleveland CC, Green PA, Holland EA, et al (2004) Nitrogen cycles: past, present, and future. *Biogeochemistry* **70**: 153–226
- Graham TR, Kozlov MM (2010) Interplay of proteins and lipids in generating membrane curvature. *Curr Opin Cell Biol* **22**: 430–436
- Heinz S, Rast A, Shao L, Gutu A, Gugel IL, Heyno E, Labs M, Rengstl B, Viola S, Nowaczyk MM, et al (2016) Thylakoid membrane architecture in *Synechocystis* depends on CurT, a homolog of the granal CURVATURE THYLAKOID1 proteins. *Plant Cell* **28**: 2238–2260
- Howard RW, Blomquist GJ (2005) Ecological, behavioral, and biochemical aspects of insect hydrocarbons. *Annu Rev Entomol* **50**: 371–393
- Howard TP, Middelhaufe S, Moore K, Edner C, Kolak DM, Taylor GN, Parker DA, Lee R, Smirnoff N, Aves SJ, et al (2013) Synthesis of customized petroleum-replica fuel molecules by targeted modification of free fatty acid pools in *Escherichia coli*. *Proc Natl Acad Sci USA* **110**: 7636–7641
- Howe CJ, Barbrook AC, Nisbet RER, Lockhart PJ, Larkum AWD (2008) The origin of plastids. *Philos Trans R Soc Lond B Biol Sci* **363**: 2675–2685
- Huang F, Parmryd I, Nilsson F, Persson AL, Pakrasi HB, Andersson B, Norling B (2002) Proteomics of *Synechocystis* sp. strain PCC 6803: identification of plasma membrane proteins. *Mol Cell Proteomics* **1**: 956–966
- Ingólfsson HI, Melo MN, van Eerden FJ, Amarez C, Lopez CA, Wassenaar TA, Periole X, de Vries AH, Tieleman DP, Marrink SJ (2014) Lipid organization of the plasma membrane. *J Am Chem Soc* **136**: 14554–14559
- Kaňa R (2013) Mobility of photosynthetic proteins. *Photosynth Res* **116**: 465–479
- Kaneko T, Sato S, Kotani H, Tanaka A, Asamizu E, Nakamura Y, Miyajima N, Hirose M, Sugiura M, Sasamoto S, et al (1996) Sequence analysis of the genome of the unicellular cyanobacterium *Synechocystis* sp. strain PCC6803. II. Sequence determination of the entire genome and assignment of potential protein-coding regions (supplement). *DNA Res* **3**: 185–209
- Kosma DK, Bourdenx B, Bernard A, Parsons EP, Lü S, Joubès J, Jenks MA (2009) The impact of water deficiency on leaf cuticle lipids of *Arabidopsis*. *Plant Physiol* **151**: 1918–1929
- Kunkel DD (1982) Thylakoid centers: structures associated with the cyanobacterial photosynthetic membrane system. *Arch Microbiol* **133**: 97–99
- Lea-Smith DJ, Biller SJ, Davey MP, Cotton CA, Perez Sepulveda BM, Turcyn AV, Scanlan DJ, Smith AG, Chisholm SW, Howe CJ (2015) Contribution of cyanobacterial alkane production to the ocean hydrocarbon cycle. *Proc Natl Acad Sci USA* **112**: 13591–13596
- Lea-Smith DJ, Bombelli P, Dennis JS, Scott SA, Smith AG, Howe CJ (2014) Pycobilisome-deficient strains of *Synechocystis* sp. PCC 6803 have reduced size and require carbon-limiting conditions to exhibit enhanced productivity. *Plant Physiol* **165**: 705–714
- Lea-Smith DJ, Bombelli P, Vasudevan R, Howe CJ (2016a) Photosynthetic, respiratory and extracellular electron transport pathways in cyanobacteria. *Biochim Biophys Acta* **1857**: 247–255
- Lea-Smith DJ, Ross N, Zori M, Bendall DS, Dennis JS, Scott SA, Smith AG, Howe CJ (2013) Thylakoid terminal oxidases are essential for the cyanobacterium *Synechocystis* sp. PCC 6803 to survive rapidly changing light intensities. *Plant Physiol* **162**: 484–495
- Lea-Smith DJ, Vasudevan R, Howe CJ (2016b) Generation of marked and markerless mutants in model cyanobacterial species. *J Vis Exp* doi/10.3791/54001
- Li N, Chang WC, Warui DM, Booker SJ, Krebs C, Bollinger JM Jr (2012) Evidence for only oxygenative cleavage of aldehydes to alk(a)enes and formate by cyanobacterial aldehyde decarbonylases. *Biochemistry* **51**: 7908–7916
- López CA, Sovova Z, van Eerden FJ, de Vries AH, Marrink SJ (2013) Martini force field parameters for glycolipids. *J Chem Theory Comput* **9**: 1694–1708
- Manna M, Róg T, Vattulainen I (2014) The challenges of understanding glycolipid functions: an open outlook based on molecular simulations. *Biochim Biophys Acta* **1841**: 1130–1145
- Marrink SJ, de Vries AH, Tieleman DP (2009) Lipids on the move: simulations of membrane pores, domains, stalks and curves. *Biochim Biophys Acta* **1788**: 149–168
- Marrink SJ, Risselada HJ, Yefimov S, Tieleman DP, de Vries AH (2007) The MARTINI force field: coarse grained model for biomolecular simulations. *J Phys Chem B* **111**: 7812–7824
- McMahon HT, Gallop JL (2005) Membrane curvature and mechanisms of dynamic cell membrane remodeling. *Nature* **438**: 590–596
- Mendez-Perez D, Begemann MB, Pfeleger BF (2011) Modular synthase-encoding gene involved in α -olefin biosynthesis in *Synechococcus* sp. strain PCC 7002. *Appl Environ Microbiol* **77**: 4264–4267

- Merzlyak MN, Naqvi KR** (2000) On recording the true absorption spectrum and the scattering spectrum of a turbid sample: application to cell suspensions of the cyanobacterium *Anabaena variabilis*. *J Photochem Photobiol B* **58**: 123–129
- Mohamed HE, Vermaas W** (2004) Slr1293 in *Synechocystis* sp. strain PCC 6803 is the C-3',4' desaturase (CrtD) involved in myxoxanthophyll biosynthesis. *J Bacteriol* **186**: 5621–5628
- Murata N, Wada H, Gombos Z** (1992) Modes of fatty-acid desaturation in cyanobacteria. *Plant Cell Physiol* **33**: 933–941
- Murphy DJ** (1982) The importance of non-planar bilayer regions in photosynthetic membranes and their stabilization by galactolipids. *FEBS Lett* **150**: 19–26
- Norling B, Zak E, Andersson B, Pakrasi H** (1998) 2D-isolation of pure plasma and thylakoid membranes from the cyanobacterium *Synechocystis* sp. PCC 6803. *FEBS Lett* **436**: 189–192
- Nürnberg DJ, Mariscal V, Parker J, Mastroianni G, Flores E, Mullineaux CW** (2014) Branching and intercellular communication in the Section V cyanobacterium *Mastigocladus laminosus*, a complex multicellular prokaryote. *Mol Microbiol* **91**: 935–949
- Porra RJ, Thompson WA, Kriedemann PE** (1989) Determination of accurate extinction coefficients and simultaneous-equations for assaying chlorophylls *a* and *b* extracted with 4 different solvents: verification of the concentration of chlorophyll standards by atomic-absorption spectroscopy. *Biochim Biophys Acta* **975**: 384–394
- Raven JA** (1998) The twelfth Tansley Lecture. Small is beautiful: the picophytoplankton. *Funct Ecol* **12**: 503–513
- Rexroth S, Mullineaux CW, Ellinger D, Sendtko E, Rögner M, Koenig F** (2011) The plasma membrane of the cyanobacterium *Gloeobacter violaceus* contains segregated bioenergetic domains. *Plant Cell* **23**: 2379–2390
- Reynolds ES** (1963) The use of lead citrate at high pH as an electron-opaque stain in electron microscopy. *J Cell Biol* **17**: 208–212
- Ried JL, Collmer A** (1987) An nptI-sacB-sacR cartridge for constructing directed, unmarked mutations in gram-negative bacteria by marker exchange- eviction mutagenesis. *Gene* **57**: 239–246
- Rippka R, Waterbury J, Cohenbazire G** (1974) Cyanobacterium which lacks thylakoids. *Arch Microbiol* **100**: 419–436
- Saw JHW, Schatz M, Brown MV, Kunkel DD, Foster JS, Shick H, Christensen S, Hou S, Wan X, Donachie SP** (2013) Cultivation and complete genome sequencing of *Gloeobacter kilauensis* sp. nov., from a lava cave in Kilauea Caldera, Hawai'i. *PLoS One* **8**: e76376
- Schirmer A, Rude MA, Li X, Popova E, del Cardayre SB** (2010) Microbial biosynthesis of alkanes. *Science* **329**: 559–562
- Sheng J, Vannella R, Rittmann BE** (2011) Evaluation of methods to extract and quantify lipids from *Synechocystis* PCC 6803. *Bioresour Technol* **102**: 1697–1703
- Shipley GG, Green JP, Nichols BW** (1973) The phase behavior of monogalactosyl, digalactosyl, and sulphoquinovosyl diglycerides. *Biochim Biophys Acta* **311**: 531–544
- Sorigué D, Légeret B, Cuiñé S, Morales P, Mirabella B, Guédeney G, Li-Beisson Y, Jetter R, Peltier G, Beisson F** (2016) Microalgae synthesize hydrocarbons from long-chain fatty acids via a light-dependent pathway. *Plant Physiol* **171**: 2393–2405
- Stengel A, Gügel IL, Hilger D, Rengstl B, Jung H, Nickelsen J** (2012) Initial steps of photosystem II de novo assembly and preloading with manganese take place in biogenesis centers in *Synechocystis*. *Plant Cell* **24**: 660–675
- Stingaciu LR, O'Neill H, Liberton M, Urban VS, Pakrasi HB, Ohl M** (2016) Revealing the dynamics of thylakoid membranes in living cyanobacterial cells. *Sci Rep* **6**: 19627
- Tan X, Yao L, Gao Q, Wang W, Qi F, Lu X** (2011) Photosynthesis driven conversion of carbon dioxide to fatty alcohols and hydrocarbons in cyanobacteria. *Metab Eng* **13**: 169–176
- Tang EPY, Peters RH** (1995) The allometry of algal respiration. *J Plankton Res* **17**: 303–315
- Tilcock CP** (1986) Lipid polymorphism. *Chem Phys Lipids* **40**: 109–125
- Valentine DL, Reddy CM** (2015) Latent hydrocarbons from cyanobacteria. *Proc Natl Acad Sci USA* **112**: 13434–13435
- van Eerden FJ, de Jong DH, de Vries AH, Wassenaar TA, Marrink SJ** (2015) Characterization of thylakoid lipid membranes from cyanobacteria and higher plants by molecular dynamics simulations. *Biochim Biophys Acta* **1848**: 1319–1330
- Vattulainen I, Rog T** (2011) Lipid simulations: a perspective on lipids in action. *Cold Spring Harb Perspect Biol* **3**: a004655
- Vieira J, Messing J** (1982) The pUC plasmids, an M13mp7-derived system for insertion mutagenesis and sequencing with synthetic universal primers. *Gene* **19**: 259–268
- White SH, King GI, Cain JE** (1981) Location of hexane in lipid bilayers determined by neutron diffraction. *Nature* **290**: 161–163
- Wu LJ, Errington J** (2011) Nucleoid occlusion and bacterial cell division. *Nat Rev Microbiol* **10**: 8–12
- Xu H, Vavilin D, Funk C, Vermaas W** (2004) Multiple deletions of small Cab-like proteins in the cyanobacterium *Synechocystis* sp. PCC 6803: consequences for pigment biosynthesis and accumulation. *J Biol Chem* **279**: 27971–27979
- Zhou X, Halladin DK, Rojas ER, Koslover EF, Lee TK, Huang KC, Theriot JA** (2015) Bacterial division. Mechanical crack propagation drives millisecond daughter cell separation in *Staphylococcus aureus*. *Science* **348**: 574–578
- Zwirgmaier K, Jardillier L, Ostrowski M, Mazard S, Garczarek L, Vault D, Not F, Massana R, Ulloa O, Scanlan DJ** (2008) Global phylogeography of marine *Synechococcus* and *Prochlorococcus* reveals a distinct partitioning of lineages among oceanic biomes. *Environ Microbiol* **10**: 147–161